Combining Short and Long Scale Effects in Modeling of Chemical-Mechanical Planarization

Sascha Bott[1], Boris Vasilev[2], Roland Rzehak[3], and Johann W. Bartha[4]

[1]Fraunhofer Institute for Photonic Microsystems (IPMS-CNT), Dresden, Germany
[2]Globalfoundries Dresden Module One LLC & Co. KG, Dresden, Germany
[3]Helmholtz-Zentrum Dresden-Rossendorf (HZDR), Dresden, Germany
[4]Institute of Semiconductor and Microsystems Technology (IHM), Dresden University of Technology, Dresden, Germany
[1]sascha.bott@cnt.fraunhofer.de

Abstract- **In chemical-mechanical planarization (CMP) chip-scale modeling is used to predict the structure height evolutions for a chip layout in combination with a certain process. Usually a test-chip is used for model calibration. The model can then be used for process optimization and control, as well as chip design support. Motivated by a demand for higher accuracy an advanced model for the simulation of the planarization behavior is proposed. It focuses on the mechanical part of CMP. Thus, roughness effects for a more accurate description of pad-wafer-contact on a short scale, which leads to an improved description of local step removal, is included. Furthermore the long scale planarization behavior depending on pattern differences in a chip and the polishing pad used, which leads to a better global step prediction, is considered. The model can be used as a foundation for future investigations on chemical influences.**

Keywords-*CMP; Chip-scale Modeling; Simulation; Interaction; Pad Roughness; Pattern Influence*

I.INTRODUCTION

Chemical-mechanical planarization (CMP) is a critical step in the fabrication of semiconductor chips. The planarity reached within a chip is vital for subsequent processing steps, especially lithography and etching. Hence if size and pattern of created structures were inaccurate, a failure of the whole chip could result. CMP planarization characterization and mathematical modeling help to understand the underlying physical and chemical mechanisms of the CMP process and can be used to improve the process performance. The layout of an integrated circuit has great influence on the successful application of a certain CMP process, as the planarization is dependent on various structural parameters like pattern-density and pattern-size. CMP models calibrated with the help of CMP test-chips can be used to predict CMP critical areas in the layout, even before the manufacturing of mask sets, and can help to reduce the costs and time-to-market.

CMP test-chips typically consist of various rather large (millimeter-sized) areas placed next to each other, each area containing a periodic line-space pattern with a certain density and pitch (see Figure 1 for definitions). The relevant range of values for the latter is between fractions of a micrometer and a few hundred micrometers.

Thus, the state-of-the-art CMP models for full-chip layout predictions are semi-empirical models that focus on previously mentioned important structural parameters like density and size [1, 2, 3, 4, 5, 6, 7, 8, 9, 10]. A combination of models and procedures that is applicable to make actual predictions for full-chip layouts [11, 12, 13, 3, 4] will be referred to as the Standard density (SD) model in the following. A detailed description can for instance be found in [5] and [10]. As the required specifications of the CMP processes increase with latest technology nodes, the CMP model accuracy also has to be improved continuously and a more detailed description of the process physics has to be incorporated.

In this paper two recently published models, the Greenwood-Williamson (GW) model [9] and the Global heights (GH) model [10], the former dealing with the influence of the pad roughness on the local planarization result and the latter with the influence of the pad bending on the global planarization, will be combined to an advanced model. The two previous models will not be discussed in detail here, however the advantages and shortcomings of both models can be briefly summarized as follows.

Greenwood-Williamson model

- effective-pattern-density and pattern-size consideration
- contact mechanics between patterned wafer and rough pad surface
- inclusion of effective curvature evolution of the contacting surfaces

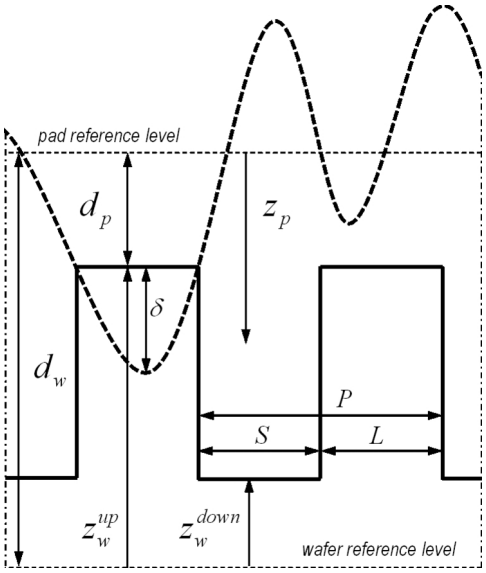

Fig. 1 Definition of structural parameters and variables for model derivation. L - line, S - Space, P - pitch, $\rho = L/P$ - density, $h = z_w^{UP} - z_w^{DOWN}$ - step height

- fast calculation

Global heights model

- dynamic structure height incorporation
- continuous long range pressure distribution
- real layout density instead of effective density
- slower iterative calculation

The strength of the Greenwood-Williamson model lies in its ability to better describe the local planarization compared to the Standard density and Global heights model, i.e. short scale effects. On the other hand, the main advantage of the Global heights model is the more accurate prediction of the global step, also expressed as total indicated range (TIR), within a chip. So the long scale effects are better incorporated compared to the Standard density and the Greenwood-Williamson model.

In the following section the derivation of the new model, which we call Roughness heights (RH) model, is shown. Basics from the Greenwood-Williamson and the Global heights model are repeated for clarification when necessary. For more details we refer to the corresponding publications.

Afterwards the models' performances are discussed by fitting to experimental process data.

Finally a summary and an outlook to future work are given.

II.ROUGHNESS HEIGHTS MODEL

For mechanically limited CMP processes, i.e. processes that can be linearly controlled by the applied nominal pressure (P_{nom}) between wafer and pad, CMP modeling focuses on the force transmission onto the wafer. The previously mentioned models all have in common, that they assume the pad-wafer-contact to be dominant for force transmission. Based on this modeling concept, for the derivation of the so-called Roughness heights model, inspired by the Greenwood-Williamson model, we will consider the pad's roughness in a shorter (μm) scale and, inspired by the Global heights model, the pad's bending capabilities, gradually following the surface of the wafer, in a longer (mm) scale.

A.Derivation for a Wafer with a Single Pattern

Due to the pad roughness only a small fraction of the pad contacts the wafer [14, 15]. For one asperity the transmission of force from pad to wafer thus can be described by the Hertzian contact theory [16]. Of course more than one asperity will come into contact in a real CMP case. With the help of the Greenwood-Williamson theory [17, 18], that introduces an asperity height distribution the Hertzian equations can be extended to describe the whole pad-wafer-contact.

Looking at an arbitrary contact of two surfaces via an area $A^\diamond$, the Greenwood-Williamson theory states, that the external force transmitted in this area, $F^\diamond$, is transmitted by $n^\diamond$ asperities having a total real contact area of $A^\diamond_{asp}$,

$$F^\diamond = \frac{E^* \sqrt{\pi}\, \sigma^{\frac{3}{2}}}{\sqrt{\kappa^\diamond}} \frac{A^\diamond N^\Phi}{A^\Phi} exp(-\frac{d_p}{\sigma}), \tag{1}$$

$$n^\diamond = \frac{A^\diamond N^\Phi}{A^\Phi} exp\left(-\frac{d_p}{\sigma}\right), \tag{2}$$

$$A^\diamond_{asp} = \frac{\pi}{\kappa^\diamond} \frac{A^\diamond N^\Phi}{A^\Phi} \sigma\, exp\,(-\frac{d_p}{\sigma}). \tag{3}$$

The external force determines the seperation d_p of the two surfaces, depending on the effective curvature of the asperities $\kappa^\diamond$, the height distribution Φ of the asperities (for CMP exponential distribution with standard deviation σ), and the effective modulus E^* of the surfaces. Note that the term $\frac{A^\diamond N^\Phi}{A^\Phi} = N^\diamond$ specifies the number of asperities present in $A^\diamond$ (not necessarily in contact).

For our special CMP case, Figure 1 shows a sketch of the pad-wafer-contact-model describing all relevant geometric parameters. Eventually, to describe the planarization behavior, the removal in up- and $down$ is of importance, thus $\diamond$ can be replaced by up and $down$, and d_p by $d_w - z_w^{up}$ and $d_w - z_w^{down}$ respectively. The resulting equations are derived in detail in Section A. In these equations the pad-wafer-distance d_w remains unknown, as F^{UP} and F^{DOWN} are not clear. However d_w can be determined by the force balance for a certain window on the wafer (A_{Window}),

$$F_{Window} = F^{UP} + F^{DOWN}. \tag{4}$$

The areas for up- and $down$-regions depend on the density inside the window.

$$A^{UP} = A_{Window}\, \rho \tag{5}$$
$$A^{DOWN} = A_{Window}\, (1 - \rho) \tag{6}$$

After a few transformations, taking into account Equations 39, 40, 5 and 6 the force balance yields

$$F_{Window} = \frac{E^* \sqrt{\pi}\, \sigma^{\frac{3}{2}}\, N^\Phi\, A_{Window}}{A^\Phi\, exp(\frac{d_w}{\sigma})} \cdot \left(\frac{\rho}{\sqrt{\kappa^{UP}}} exp\left(\frac{z_w^{UP}}{\sigma}\right) + \frac{(1-\rho)}{\sqrt{\kappa^{DOWN}}} exp\left(\frac{z_w^{DOWN}}{\sigma}\right)\right). \tag{7}$$

The term in the right hand parentheses includes all structural parameters on the wafer side and is therefore named SP'.

$$SP' = \left(\frac{\rho}{\sqrt{\kappa^{UP}}} exp\left(\frac{z_w^{UP}}{\sigma}\right) + \frac{(1-\rho)}{\sqrt{\kappa^{DOWN}}} exp\left(\frac{z_w^{DOWN}}{\sigma}\right)\right) \tag{8}$$

It shows all pattern parameters that influence the planarization behavior — density, heights and curvatures, which are step and structure size dependent.

Equation 7 can now be adjusted to

$$F_{Window} = \frac{E^* \sqrt{\pi}\, \sigma^{\frac{3}{2}}\, N^\Phi\, A_{Window}}{A^\Phi\, exp(\frac{d_w(x,y)}{\sigma})}\, SP'(x,y), \tag{9}$$

and the pad-wafer-distance d_w can be determined

$$d_w = \sigma\, ln\left[\frac{E^* \sqrt{\pi}\, \sigma^{\frac{3}{2}}\, N^\Phi\, A_{Window}}{A^\Phi\, F_{Window}}\, SP'(x,y)\right]. \tag{10}$$

With an expression for the pad distance it is possible to calculate the removal rates for the up- and $down$-regions. For this one has to keep in mind, that the pad does not contact the whole (projected) wafer surface, thus

$$A^{UP}_{asp} \neq A^{UP}, \qquad A^{DOWN}_{asp} \neq A^{DOWN}. \tag{11}$$

From the modeling point of view material removal only occurs where pad and wafer are in contact. Therefore it is useful to calculate the mean volumetric removal rate of an asperity first [19],

$$\overline{VRR_{asp}^{UP}} = k' v \frac{F^{UP}}{A_{asp}^{UP}}, \qquad \overline{VRR_{asp}^{DOWN}} = k' v \frac{F^{DOWN}}{A_{asp}^{DOWN}}. \tag{12}$$

The overall volume removed by the contacting asperities per unit time and area on the wafer equals the commonly used removal rate

$$RR^{UP} = \overline{VRR_{asp}^{UP}} \frac{n^{UP}}{A^{UP}}, \qquad RR^{DOWN} = \overline{VRR_{asp}^{DOWN}} \frac{n^{DOWN}}{A^{DOWN}}, \tag{13}$$

hence

$$RR^{UP} = k' v \frac{F^{UP}}{A_{asp}^{UP}} \frac{n^{UP}}{A^{UP}}, \tag{14}$$

$$RR^{DOWN} = k' v \frac{F^{DOWN}}{A_{asp}^{DOWN}} \frac{n^{DOWN}}{A^{DOWN}}. \tag{15}$$

At this stage the parameter k' remains unknown. The Preston coefficient k_{Pr} can be obtained from polishing experiments on blanket wafers. Therefore comparing the removal rate on a blanket wafer obtained by the Greenwood-Williamson theory,

$$RR = \overline{VRR_{asp}} \frac{n^{Wafer}}{A^{Wafer}}, \tag{16}$$

$$= k' v \frac{\kappa_{asp}}{\pi \sigma} \frac{F^{Wafer}}{A^{Wafer}}, \tag{17}$$

with the removal rate obtained through the Preston equation

$$RR = k_{Pr} v \frac{F_{Wafer}}{A_{Wafer}}, \tag{18}$$

yields

$$k' = \frac{k_{Pr} \pi \sigma}{\kappa_{asp}}. \tag{19}$$

Again, for more details follow the derivations in Section A. In summary the final equations for the removal rates in up and $down$ are obtained,

$$RR^{UP} = k_{Pr} v \frac{\sqrt{\kappa^{UP}}}{\kappa_{asp}} \frac{F_{Window}}{A_{Window}} \frac{exp(\frac{z_w^{UP}}{\sigma})}{SP'}, \tag{20}$$

$$RR^{DOWN} = k_{Pr} v \frac{\sqrt{\kappa^{DOWN}}}{\kappa_{asp}} \frac{F_{Window}}{A_{Window}} \frac{exp(\frac{z_w^{DOWN}}{\sigma})}{SP'}. \tag{21}$$

B.Incorporation of Pattern Interaction

Equations 20 and 21 can be used on a wafer that is patterned with a single type of structure. For a perfect CMP process, the planarization behavior is the same everywhere on the wafer or in the chip, therefore lateral interaction is not accounted for. However of course usually a combination of different patterns is present within one chip. It is well-known that these patterns influence each other [12, 20, 4, 21, 22, 5]. This interaction is attributed to the pad which gradually follows the surface. It can also be thought of the force transmission being determined by a certain area around a place (x,y) looked at. This is also imaginable as only a few percent of the pad actually touches the wafer. Thus the mean pad-wafer-distance at a specific place (x,y) will be determined by the place itself but also by the impact of the surrounding. The further away from the place of interest the less the contribution will be to the force balance. Inversely the pad-wafer-distance directly affects the force transmitted at place (x,y).

So the pad-wafer-distance d_w changes within the chip depending on the place (x,y) and naturally it does not change abruptly. Such a behavior can be described by a response function of the pad. Usually a Gaussian weighting function with the interaction length IL as the standard deviation is used as an approximation.

$$w(x, x', y, y') = \frac{1}{2\pi(IL)^2} exp\left(-\frac{(x-x')^2 + (y-y')^2}{2(IL)^2}\right) \tag{22}$$

The structures together with the pad asperities determine the force transmitted. As the pad asperities do not change within the chip the structural parameters, combined in the parameter SP' in Equation 8, are weighted,

$$SP(x,y) \;=\; \int_{x'} \int_{y'} w(x,x',y,y')\, SP'(x',y')\, dx'\, dy',. \tag{23}$$

With this the pad-wafer-distance is calculated,

$$d_w(x,y) \;=\; \sigma\, ln \left[\frac{E^*\, \sqrt{\pi}\, \sigma^{\frac{3}{2}}\, N^{\Phi}\, A^{Window}}{A^{\Phi}\, F^{Window}}\, SP(x,y) \right]. \tag{24}$$

This will eventually result in the adjusted equations for the removal rates,

$$RR^{UP} \;=\; k_{Pr}\, v\, \frac{\sqrt{\kappa^{UP}}}{\kappa_{asp}}\, \frac{F_{Window}}{A_{Window}}\, \frac{exp(\frac{z_w^{UP}}{\sigma})}{SP}, \tag{25}$$

$$RR^{DOWN} \;=\; k_{Pr}\, v\, \frac{\sqrt{\kappa^{DOWN}}}{\kappa_{asp}}\, \frac{F_{Window}}{A_{Window}}\, \frac{exp(\frac{z_w^{DOWN}}{\sigma})}{SP}. \tag{26}$$

With Equations 25 and 26 the desired height evolutions

$$\frac{dz_w^{\diamond}}{dt} \;=\; -RR^{\diamond}, \tag{27}$$

can be calculated with a simple Euler-algorithm.

In the Greenwood-Williamson theory, from a mathematical point of view, every place on a wafer surface is in contact with the pad, due to the exponential height distribution of the pad asperities. Because of this, the derived model has a non-iterative structure, as compared to the Global heights model [10], in which for the force balance first the question of contact has to be evaluated, which in turn depends on the force balance. Therefore calculation times for the Roughness heights model are much smaller, more precisely in the order of the Standard density or Greenwood-Williamson model, i.e. a few seconds for a usual test-chip case.

III.EXPERIMENTS AND DISCUSSION

The model performance is judged by comparing fit values of the established models with the new model and by comparing the corresponding plots of the global and local steps for a known set of data [10].

In this experiment planarization runs have been carried out on 300-mm-wafers having gone through a typical shallow trench isolation (STI) process. A silicon nitride layer of about 150 nm thickness was deposited on blanket wafers. A test mask containing patches of line-space structures with a density ranging from 4 % to 72 % at a pitch of 250 μm, as shown in Figure 2, was used to lithographically pattern the wafer. After dry-etching the trenches to a depth of roughly 365 nm, about 880 nm silicon oxide

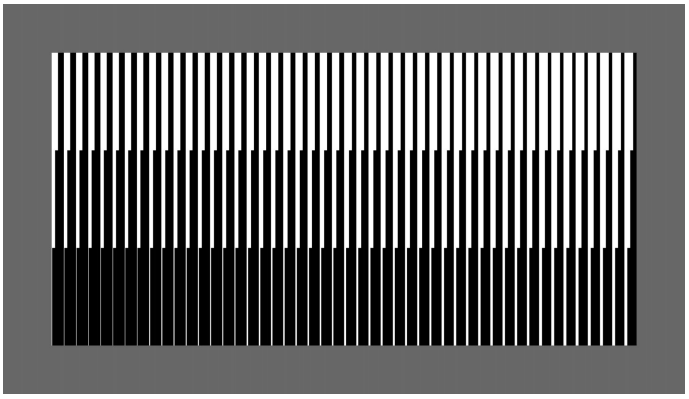

Fig. 2 Test mask / structures used for experiment; 18 patches with 250 μm pitch and densities ranging from 4 % to 72 % in steps of 4 %; white: up-regions; black: $down$-regions; grey: unresolved.

was deposited by a high density plasma (HDP) process. For the CMP process an AMAT Reflexion LK polisher was used. The experiments were carried out on a single platen fitted with a k-grooved IC1010 pad. Conditioning was done in situ with a Kinik

3BG conditioner and a downforce of $7\,lbf$. The nominal pressure was $19.3\,kPa$, the platen speed $63\,rpm$ and the carrier speed $62\,rpm$. A Klebosol slurry was supplied at a flow rate of $250\,ml\,min^{-1}$. In the experiments, one separate wafer was used for each process point in time. After the process, reflectometry measurements were made to determine the layer thicknesses in up- and $down$-regions in the center of each density patch. Together with the initial step-height determined from profiler scans before the process, absolute heights above some reference level were calculated. All data was collected on the chip closest to the center of the wafer.

The exact fit strategy is explained in [10]. Summarized, when fitting the data emphasis has been put on a good TIR fit, while maintaining acceptable absolute and relative fits of the up-, $down$- and step-height. Table 1 shows the fitted model parameters and the resulting rms-deviations between experiment and simulation.

TABLE 1 PARAMETER VALUES FOR MODEL FITS TO DATA; RH: ROUGHNESS HEIGHTS MODEL GH: GLOBAL HEIGHTS MODEL; SD: STANDARD DENSITY MODEL.

model type	RH	GH	GW	SD
RR_{Oxide}	$2.99\,nms^{-1}$	$3.02\,nms^{-1}$	$2.98\,nms^{-1}$	$3.02\,nms^{-1}$
$RR_{Nitride}$	$1.32\,nms^{-1}$	$1.32\,nms^{-1}$	$1.31\,nms^{-1}$	$1.35\,nms^{-1}$
E	–	$170\,MPa$	–	$160\,MPa$
σ	$145\,nm$	–	$145\,nm$	–
α	5	–	5	–
IL	$1300\,\mu m$	$1250\,\mu m$	$2800\,\mu m$	$2050\,\mu m$
rms-deviations simulation — experiment				
TIR local steps planarized (i.e. $h(x,y) \approx 0\,\forall\,(x,y)$)	$2.6\,nm$	$3.1\,nm$	$31.0\,nm$	$19.5\,nm$
TIR w/o dishing phase	$4.0\,nm$	$4.5\,nm$	$20.7\,nm$	$16.9\,nm$
TIR all phases	$5.2\,nm$	$5.2\,nm$	$27.4\,nm$	$21.1\,nm$
up- and step-height all densities	$15.0\,nm$	$20.7\,nm$	$13.9\,nm$	$22.6\,nm$

We discuss the standard density model first. It is based on the assumption that the pad can be described by laterally independent Hookean springs. Additionally, the long scale pad bending effects are described by weighing the layout density with a Gaussian filter function once at the beginning of the simulation. This results in an average fit quality concerning the rms-deviations of both global step (TIR) and height values. Figure 3 shows the TIR evolution in the course of the process. Especially

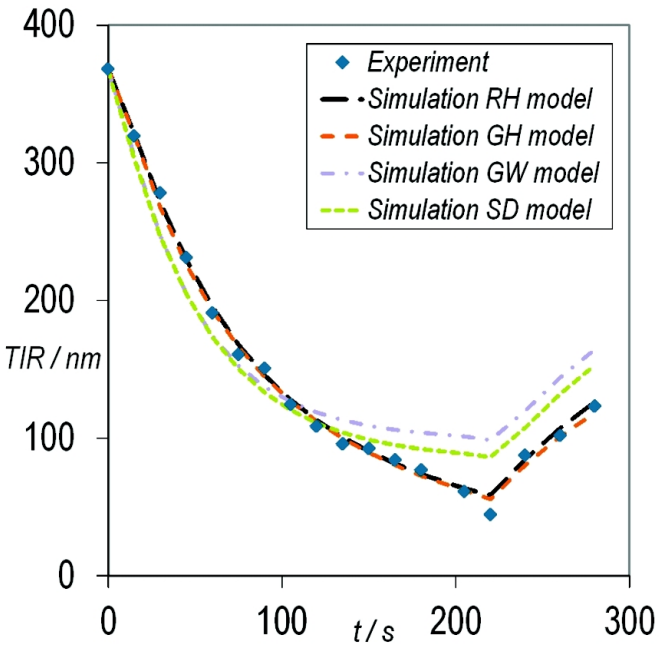

Fig. 3 Comparison of experimentally measured TIR (symbols) to model predictions (lines) with best fit to data of all phases

when trying to best fit the TIR in all process phases from beginning until local planarization, i.e. $h(x, y) \approx 0$ everywhere, the SD model's TIR deviation is highest for the time when the planarization process ought to be stopped, just before the step is increasing again. Table 1 shows that the Greenwood-Williamson model is similarly bad in predicting the TIR. However, here, the TIR values are even worse as a trade-off for improved overall height predictions. The local heights prediction is the strength of the GW model due to its incorporation of pad roughness parameters. However the long scale effects are not treated with the necessary accuracy. On the other hand the TIR prediction can substantially be improved with the Global heights model, which introduces a permanent reevaluation of the force balance over time resulting in permanent pressure redistribution within the chip. The overall height predictions are hardly affected compared to the standard density model. Furthermore the prediction of the local steps is poor, cf. Figure 4.

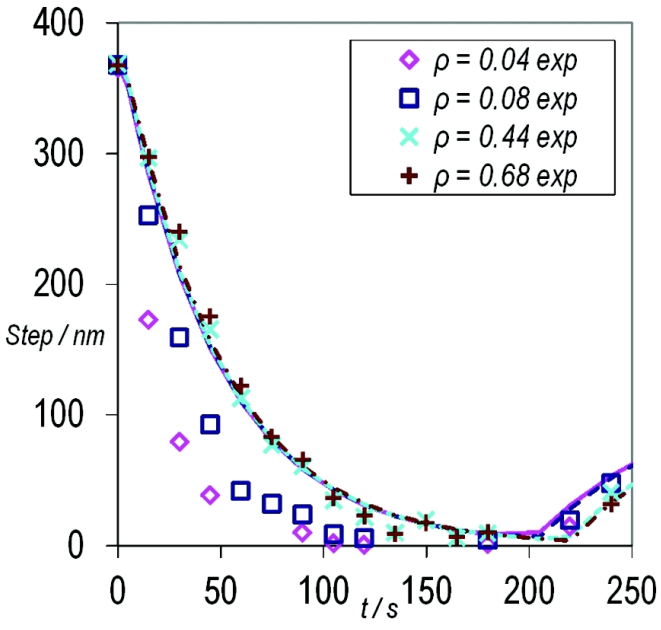

Fig. 4 Local step height evolution for various density patches - experiment (symbols) and simulated by Global heights model (lines)

As desired, the Roughness heights model picks up the strengths of both GW and GH models and leads to an excellent prediction of the TIR together with an improved local height prediction. Figure 5 additionally shows the qualitatively improved fit for local steps.

In summary the new model advances the description of the mechanical part of chemical-mechanical planarization. The improved fit quality supports the theses of both pad roughness and deflection influences.

With such an improved mechanical model it is possible to address sophisticated effects, like threshold pressure or adsorption mechanisms. It is especially easier to separate chemical from mechanical effects. More mathematically speaking, on one hand, one could either include different non-linear wear laws directly. For example the Preston equation could be changed from its standard form to an often experimentally obtained potential form

$$RR = k_{Pr}\, v\, P_{nom}^{a}. \tag{28}$$

On the other hand a non-linear behavior could result from a more complex wear law, in which the pressure is only one key aspect. Rather than calculating the actual removal rates, the main purpose of the model should be seen in generating a pressure field for the chip area. The pressure can contribute to the process in one way or another. As we have used Preston's law, dividing Equations 25 and 26 by the Preston coefficient and the relative velocity, $k_p\, v$, results in the expressions for the time-averaged mean up- and $down$-pressures on the structures.

$$P^{UP} = \frac{\sqrt{\kappa^{UP}}}{\kappa_{asp}} \frac{F^{Window}}{A^{Window}} \frac{exp(\frac{z_{GH}^{UP}}{\sigma})}{SP} \tag{29}$$

$$P^{DOWN} = \frac{\sqrt{\kappa^{DOWN}}}{\kappa_{asp}} \frac{F^{Window}}{A^{Window}} \frac{exp(\frac{z_{GH}^{DOWN}}{\sigma})}{SP} \tag{30}$$

These equations could for example be used for a Preston-like wear law with time dependent Preston coefficient, as one example for chemical effects.

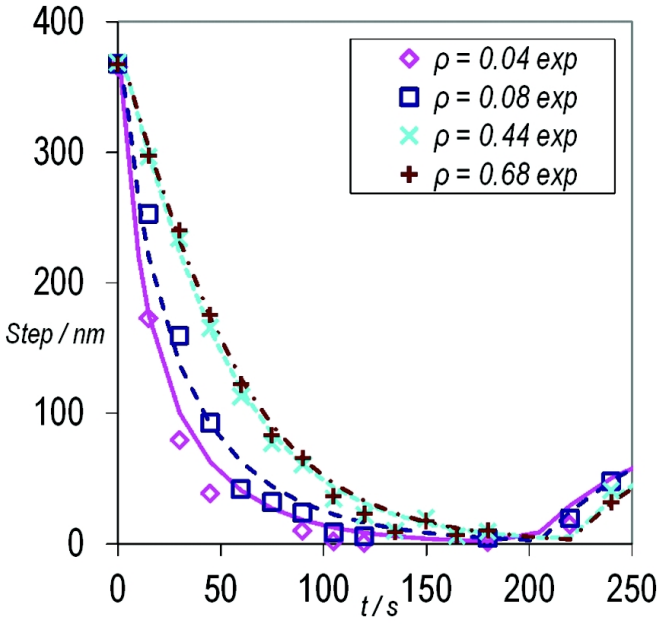

Fig. 5 Local step height evolution for various density patches - experiment (symbols) and simulated by Roughness heights model (lines)

IV.CONCLUSION

A new chip-scale CMP model has been proposed, which combines short scale effects, by accounting for pad roughness and more detailed structural parameters, as well as long scale effects, like pad deflection and surrounding structural support, in the planarization process. It is thus possible to simulate the mechanical contribution on the planarization behavior with a higher accuracy for local structures and globally within a chip.

The model foundation itself has turned away from the elastic Hookean spring assumption, as in the Standard density and Global heights model, towards a description of the pad-wafer-contact through roughness, more precisely pad asperities and wafer feature shapes. Compared to the Greenwood-Williamson model, that is already based on the roughness idea, the description of the interaction between different regions within a chip is improved by continuously weighing the force transmission with a filter function, which contains the fit parameter IL. It is well-known, that different pad conditions will influence the long range interaction, thus IL will be a function of the pad parameters, especially elastic modulus and thickness, which determine its deflection capabilities. It is now possible to systematically investigate the influence of these parameters on IL and thus TIR - a measure for the important within-chip non-uniformity, for so-called mechanically dominated processes. Together with defectivity data and pad life time analyses this could yield valuable information for choosing the right consumable set for a certain CMP integration step. Concerning planarization behavior and pad life time, the model could also be used to help analyse the impact of different pad roughnesses, generated by different conditioning setups [23]. Furthermore, the model basics can be used to address non-linear CMP processes (so-called chemically-dominated), like STI polish with ceria slurry, in which additives play a key role and the removal is no longer directly proportional to the applied pressure, but still pressure dependent. Of course, the model basics could also be extended to other processes like copper and barrier polish.

ACKNOWLEDGMENTS

This work was supported in part by the Federal Ministry of Education and Research of the Federal Republic of Germany, under Project Number 13N10808.

A.DETAILED MODEL DERIVATION

The Hertzian contact [16] of one pad asperity

$$n_{asp} \;=\; 1, \tag{31}$$

results in the force transmitted by that asperity

$$F_{asp} \;=\; \frac{4}{3}\,\frac{E^*}{\sqrt{\kappa}}\,\delta^{\frac{3}{2}}, \tag{32}$$

through the contact area between asperity and wafer surface

$$A_{asp} \;=\; \frac{\pi}{\kappa}\,\delta\,. \tag{33}$$

Here E^* is the effective elastic modulus, κ the effective curvature of the contacting surfaces and δ the resulting compression of the asperity.

The Greenwood-Williamson theory [17, 18] introduces an asperity height distribution to describe a rough surface, where N^Φ is the maximum possible number of asperities that can come into contact with the wafer, measured on a sample with the area A^Φ,

$$\Phi(z_{pad}) \;=\; N^\Phi\,\frac{1}{\sigma}\,exp(-\frac{z_{pad}}{\sigma}) \qquad\qquad z_{pad} \geq 0. \tag{34}$$

The asperity compression can be written as (cf. Figure 1)

$$\delta \;=\; z_{pad} \;-\; d_{pad}. \tag{35}$$

Incorporating the asperity height distribution from Equation 34, the force $F^\diamond$ transmitted by all asperities in a certain area $A^\diamond$ is

$$F^\diamond \;=\; \frac{4}{3}\,\frac{E^*}{\sqrt{\kappa^\diamond}}\,\frac{A^\diamond}{A^\Phi}\int_{d_{pad}}^{\infty}(z_{pad}-d_{pad})^{\frac{3}{2}}\,\Phi(z_{pad})\,dz_{pad}, \tag{36}$$

$$\;=\; \frac{E^*\,\sqrt{\pi}\,\sigma^{\frac{3}{2}}}{\sqrt{\kappa^\diamond}}\,\frac{A^\diamond\,N^\Phi}{A^\Phi}\,exp(-\frac{d_{pad}}{\sigma}). \tag{37}$$

Of interest are the wafer, for blanket removal considerations, as well as the UP- and $DOWN$-regions. Table **??** shows, what the general parameters look like for these cases.

$\diamond$	$F^\diamond$	$A^\diamond$	$\kappa^\diamond$	d_{pad}
$Wafer$	F^{Wafer}	A^{Wafer}	κ_{asp}	d_{pad}
UP	F^{UP}	A^{UP}	κ^{UP}	$d_w - z_w^{UP}$
$DOWN$	F^{DOWN}	A^{DOWN}	κ^{DOWN}	$d_w - z_w^{DOWN}$

Thus the force transmitted onto a blanket wafer through the pad's asperities is

$$F^{Wafer} \;=\; \frac{E^*\,\sqrt{\pi}\,\sigma^{\frac{3}{2}}}{\sqrt{\kappa_{asp}}}\,\frac{A^{Wafer}\,N^\Phi}{A^\Phi}\,exp(-\frac{d_{pad}}{\sigma}), \tag{38}$$

onto the UP-structures in a test-chip

$$F^{UP} \;=\; \frac{E^*\,\sqrt{\pi}\,\sigma^{\frac{3}{2}}\,N^\Phi}{A^\Phi}\,\frac{A^{UP}}{\sqrt{\kappa^{UP}}}\,\frac{exp\,(\frac{z_w^{UP}}{\sigma})}{exp(\,\frac{d_w}{\sigma})}, \tag{39}$$

and onto the $DOWN$-structures in that chip

$$F^{DOWN} \;=\; \frac{E^*\,\sqrt{\pi}\,\sigma^{\frac{3}{2}}\,N^\Phi}{A^\Phi}\,\frac{A^{DOWN}}{\sqrt{\kappa^{DOWN}}}\,\frac{exp\,(\frac{z_w^{DOWN}}{\sigma})}{exp(\,\frac{d_w}{\sigma})}. \tag{40}$$

Furthermore the number of asperities contacting in area $A^{\diamond}$ is

$$n^{\diamond} = \frac{A^{\diamond}}{A^{\Phi}} \int_{d_{pad}}^{\infty} \Phi(z_{pad})\, dz_{pad}, \tag{41}$$

$$= \frac{A^{\diamond}\, N^{\Phi}}{A^{\Phi}}\, exp\left(-\frac{d_{pad}}{\sigma}\right). \tag{42}$$

Thus, the number of contacting asperities depending on pad-wafer-distance d_{pad} for a blanket wafer is

$$n^{Wafer} = \frac{A^{Wafer}\, N^{\Phi}}{A^{\Phi}}\, exp(-\frac{d_{pad}}{\sigma}). \tag{43}$$

The number of contacting asperities in the UP-region is

$$n^{UP} = \frac{A^{UP}\, N^{\Phi}}{A^{\Phi}}\, \frac{exp\,(\frac{z_w^{UP}}{\sigma})}{exp(\,\frac{d_w}{\sigma})}, \tag{44}$$

and the number of contacting asperities in the $DOWN$-region is

$$n^{DOWN} = \frac{A^{DOWN}\, N^{\Phi}}{A^{\Phi}}\, \frac{exp\,(\frac{z_w^{DOWN}}{\sigma})}{exp(\,\frac{d_w}{\sigma})}. \tag{45}$$

Starting from Equation 33 the contacting area of all asperities can be written as

$$A_{asp}^{\diamond} = \frac{\pi}{\kappa^{\diamond}}\, \frac{A^{\diamond}}{A^{\Phi}} \int_{d_{pad}}^{\infty} (z_{pad} - d_{pad})\, \Phi(z_{pad})\, dz_{pad}. \tag{46}$$

The contact area of the asperities on a blanket wafer is

$$A_{asp}^{Wafer} = \frac{\pi}{\kappa_{asp}}\, \frac{A^{Wafer}\, N^{\Phi}}{A^{\Phi}}\, \sigma\, exp\,(-\frac{d_{pad}}{\sigma}), \tag{47}$$

the contact area in the UP-region is

$$A_{asp}^{UP} = \frac{\pi}{\kappa^{UP}}\, \frac{A^{UP}\, N^{\Phi}}{A^{\Phi}}\, \sigma\, \frac{exp\,(\frac{z_w^{UP}}{\sigma})}{exp(\,\frac{d_w}{\sigma})}, \tag{48}$$

an analog for the $DOWN$-region is

$$A_{asp}^{DOWN} = \frac{\pi}{\kappa^{DOWN}}\, \frac{A^{DOWN}\, N^{\Phi}}{A^{\Phi}}\, \sigma\, \frac{exp\,(\frac{z_w^{DOWN}}{\sigma})}{exp(\,\frac{d_w}{\sigma})}. \tag{49}$$

From these basic expressions some furhter values can be calculated.

Force and number of asperities together give the mean force transmitted by one asperity, for a blanket wafer

$$\overline{F^{Wafer}} = \frac{F^{Wafer}}{n^{Wafer}} = \frac{E^*\sqrt{\pi}\sigma^{\frac{3}{2}}}{\sqrt{\kappa_{asp}}}, \tag{50}$$

and for the up- and $down$-region

$$\overline{F^{UP}} = \frac{F^{UP}}{n^{UP}} = \frac{E^*\sqrt{\pi}\sigma^{\frac{3}{2}}}{\sqrt{\kappa^{UP}}}, \qquad \overline{F^{DOWN}} = \frac{E^*\sqrt{\pi}\sigma^{\frac{3}{2}}}{\sqrt{\kappa^{DOWN}}}. \tag{51}$$

The mean contact area of one asperity contacting the blanket wafer becomes

$$\overline{A_{asp}^{Wafer}} = \frac{A_{asp}^{Wafer}}{n^{Wafer}} = \frac{\pi\sigma}{\kappa_{asp}}, \tag{52}$$

the mean contact area of one asperity contacting the UP-region, respectively the $DOWN$-region

$$\overline{A_{asp}^{UP}} = \frac{A_{asp}^{UP}}{n^{UP}} = \frac{\pi\sigma}{\kappa^{UP}}, \qquad \overline{A_{asp}^{DOWN}} = \frac{A_{asp}^{DOWN}}{n^{DOWN}} = \frac{\pi\sigma}{\kappa^{DOWN}}. \tag{53}$$

Thus the mean pressure under one asperity contacting the blanket wafer is

$$\overline{P_{asp}^{Wafer}} = \frac{\overline{F^{Wafer}}}{\overline{A_{asp}^{Wafer}}} = \frac{E^* \sqrt{\sigma} \sqrt{\kappa_{asp}}}{\sqrt{\pi}}, \tag{54}$$

in UP-region and $DOWN$-region

$$\overline{P_{asp}^{UP}} = \frac{E^* \sqrt{\sigma} \sqrt{\kappa^{UP}}}{\sqrt{\pi}}, \qquad \overline{P_{asp}^{DOWN}} = \frac{E^* \sqrt{\sigma} \sqrt{\kappa^{DOWN}}}{\sqrt{\pi}}. \tag{55}$$

The mean pressure under one asperity is used to calculate the mean volumetric removal rate [19] on a blanket wafer.

$$\overline{VRR_{asp}^{Wafer}} = k' \, v \, \overline{P_{asp}^{Wafer}} \tag{56}$$

The blanket removal rate on the wafer is

$$RR = \overline{VRR_{asp}} \, \frac{n^{Wafer}}{A^{Wafer}}, \tag{57}$$

$$= k' \, v \, \frac{\kappa_{asp}}{\pi \, \sigma} \, \frac{F^{Wafer}}{A^{Wafer}}, \tag{58}$$

which can also be described by the Preston equation

$$RR = k_{Pr} \, v \, P_{nom}. \tag{59}$$

Comparing the equations, with $P_{nom} = \frac{F^{Wafer}}{A^{Wafer}}$ yields

$$k_{Pr} = k' \, \frac{\kappa_{asp}}{\pi \, \sigma}, \qquad k' = \frac{k_{Pr} \, \pi \, \sigma}{\kappa_{asp}}. \tag{60}$$

The Preston coefficient k_{Pr} together with the relative velocity v can be obtained from polishing experiments on blanket wafers.

To reach the final equations for the removal rates in up and $down$ the force balance from Section II. has to be applied to calculate the pad-wafer-distance. Furthermore the therein obtained surface parameter SP' has to be weighted to include long range effects, giving SP. Similarly to a blanket wafer the removal rate for the up-region is reached via the volumetric removal rate and eventually yields

$$RR^{UP} = k_{Pr} \, v \, \frac{\sqrt{\kappa^{UP}}}{\kappa_{asp}} \, \frac{F^{Window}}{A^{Window}} \, \frac{exp(\frac{z_w^{UP}}{\sigma})}{SP}. \tag{61}$$

Analogous for the $DOWN$-region the removal rate is

$$RR^{DOWN} = k_{Pr} \, v \, \frac{\sqrt{\kappa^{DOWN}}}{\kappa_{asp}} \, \frac{F^{Window}}{A^{Window}} \, \frac{exp(\frac{z_w^{DOWN}}{\sigma})}{SP}. \tag{62}$$

REFERENCES

[1] B. E. Stine, D. O. Ouma, R. R. Divecha, D. S. Boning, J. E. Chung, D. L. Hetherington, C. R. Harwood, O. S. Nakagawa, and S.-Y. Oh. Rapid characterization and modeling of pattern-dependent variation in chemical-mechanical polishing. *IEEE Transactions on Semiconductor Manufacturing*, 11:129–140, February 1998.

[2] D. Ouma, D. Boning, J. Chung, G. Shinn, L. Olsen, and J. Clark. An integrated characterization and modeling methodology for CMP dielectric planarization. *IITC*, page 67, 1998. elliptic weighting function, effective density.

[3] Taber H. Smith, Simon J. Fang, Duane S. Boning, Greg B. Shinn, and Jerry A. Stefani. A CMP model combining density and time dependencies. *CMPMIC*, page 97, 1999.

[4] D. Okumu Ouma, Duane S. Boning, James E. Chung, William G. Easter, Vivek Saxena, Sudhanshu Misra, and Annette Crevasse. Characterization and modeling of oxide chemical-mechanical polishing using planarization length and pattern density concepts. *IEEE Transcations on Semiconductor Manufacturing*, 15:232, 2002.

[5] R. Rzehak. Modeling pattern effects in oxide CMP. *MRS Proc*, 867:W5.10, 2005.

[6] R. Rzehak. Pitch-dependence in oxide CMP. *CMPMIC*, page 137, 2006.

[7] Roland Rzehak and Boris Vasilev. Greenwood-Williamson model for pattern-dependent planarization. *ICPT*, page 195, 2007.

[8] Xiaoping Wang, Pavan Karra, Abhijit Chandra, and Ashraf F. Bastawros. A multi-scale model for wafer surface evolution in chemical mechanical planarization (CMP). *ISEM*, 2007.

[9] Boris Vasilev, Roland Rzehak, Sascha Bott, Peter Kuecher, and Johann W. Bartha. Greenwoodwilliamson model combining pattern-density and pattern-size effects in CMP. *IEEE Transactions on Semiconductor Manufacturing*, 24(2):338–347, May 2011.

[10] Sascha Bott, Roland Rzehak, Boris Vasilev, Peter Kuecher, and Johann W. Bartha. A CMP model including global distribution of pressure. *IEEE Transactions on Semiconductor Manufacturing*, 24(2):304–314, May 2011.

[11] E. Tseng, C. Yi, and H. C. Chen. A mechanical model for DRAM dielectric CMP process. *CMPMIC*, page 258, 1997.

[12] B. Stine, D Ouma, R. Divecha, D. Boning, and J. Chung. A closed-form analytic model for ILD thickness variation in CMP processes. *CMPMIC*, page 266, 1997.

[13] J. Grillaert, M. Meuris, E. Vrancken, N. Heylen, K. Devriendt, and M. Heyns. Modelling step height reduction and local removal rates based on pad-substrate interactions. *CMPMIC*, page 79, 1998.

[14] Carolina L. Elmufdi and Gregory P. Muldowney. A novel optical technique to measure pad-wafer contact area in chemical mechanical planarization. *MRS Proc.*, 914:F12.6, 2006.

[15] C. L. Elmufdi and G. P. Muldowney. The impact of diamond conditioning on surface contact in CMP pads. *Mater. Res. Soc. Symp. Proc.*, 991, 2007.

[16] H. Hertz. Über die Berührung fester elastischer Körper. *Journal für die reine und angewandte Mathematik*, 92:156–171, 1881.

[17] J.A. Greenwood and J.B.P. Williamson. Contact of nominally flat surfaces. *Proc. R. Soc. London*, 1966.

[18] K.L. Johnson. *Contact Mechanics*. Cambridge University Press, 1985.

[19] J. F. Archard. Contact and rubbing of flat surfaces. *Journal of Applied Physics*, 24(8):981–988, August 1953.

[20] D. Boning, B. Lee, C. Oji, D. Ouma, T. Park, T. Smith, and T. Tugbawa. Pattern dependent modeling for CMP optimization and control. *MRS Proc.*, 566:197, 2000. removal-rate diagram.

[21] Johann. W. Bartha, Tilo Bormann, Kathrin Estel, and Dieter Zeidler. Assessment of planarization length variation by the step-polish-response (SPR) method. *MRS Proc.*, 816:K8.5, 2004.

[22] Jihong Choi and David A. Dornfeld. Modeling of pattern density dependent pressure non-uniformity at a die scale for ILD chemical mechanical planarization. *MRS Proc.*, 816:K4.4, 2004.

[23] Boris Vasilev, Sascha Bott, Roland Rzehak, Romy Liske, and Johann W. Bartha. A method for characterizing the pad surface texture and modeling its impact on the planarization in CMP. *Microelectron. Eng.*, 104:48–57, April 2013.